Micropolar peridynamic modeling of concrete structures

W. Gerstle, N. Sau, & E. Aguilera
Department of Civil Engineering, University of New Mexico, Albuquerque, NM, USA

ABSTRACT: The peridynamic model described in (Silling 1998; Gerstle et al. 2005), being a central-force model, is limited to modeling materials with a Poisson's ratio of one-quarter. In this paper, the peridynamic model is generalized by adding peridynamic moments to simulate linear elastic materials with varying Poisson's ratios. This micropolar peridynamic model is placed within a finite element context to enable efficacious application of boundary conditions and efficient computational solutions using an implicit, rather than an explicit, solution algorithm. The algorithm is suitable for quasistatic simulation of damage and cracking in concrete structures.

Very simple constitutive models at the peridynamic level appear to be sufficient to model the complex damage and fracture phenomena observed in concrete structures.

The peridynamic model predicts significant elastic boundary effects that are not predicted by classical stress-strain models. As a consequence, the peridynamic model predicts an effect of specimen size upon elastic stiffness.

1 INTRODUCTION

The micropolar peridynamic model has been introduced in (Gerstle et al. 2007). In essence, this model assumes an infinite number of infinitesimal frame elements (of finite length) connect infinitesimally-sized material particles together. We call these infinitesimal frame elements "micropolar peridynamic links". The infinitesimal material particles move in accordance with Newton's Second Law in response to both external forces and internal forces which result from the deformations and rotations of the ends of the peridynamic links.

Lattice models of materials, for example (Schlangen & Van Mier 1992), are not new. What is new with the micropolar peridynamic model is the idea that these lattice models can be extended into the infinitesimal regime, and that the material properties can be expressed independently of the method in which these lattice models are discretized (Gerstle, et al. 2007).

Silling (Silling 2002) has developed a peridynamic computer program, called EMU, which assumes material particles are rigid bodies of finite, rather than infinitesimal, size. This modeling assumption requires a huge number of such material particles even for modeling relatively simple structures. (Gerstle et al. 2007) have shown how the micropolar peridynamic model can be implemented within a finite element framework. This finite element implementation of the micropolar peridynamic model can drastically reduce the number of degrees of freedom required to represent a structural model.

The great advantage of the peridynamic model is that discontinuous displacement fields can emerge as the peridynamic links weaken and are broken. Indeed, the initial continuous displacement field is also an emergent, rather than a pre-assumed, phenomenon.

We present here a very simple micropolar peridynamic model that is capable of accurately modeling failure of a uniaxial concrete specimen in both tension and in compression as well as in a number of other stress states.

The micropolar peridynamic model produces some surprising behavior that is not predicted by the classical theory of elasticity. For example, this nonlocal model predicts a flexible boundary layer and a consequent size effect on elastic behavior for small structural sizes. These effects are discussed in this paper.

2 MICROPOLAR PERIDYNAMIC MODEL

The micropolar peridynamic model is able to model concrete and other quasibrittle materials with Poisson's ratios having values different than ¼. By allowing moments and rotations in addition to forces and displacements, the micropolar peridynamic model is a generalization of Silling's peridynamic model (Silling: 1998; 2000; 2002). This model is placed in a finite element framework, which allows effective application of boundary conditions, where the displacement field contained in each element is assumed to be continuous and high strain gradients or discontinuities can develop between elements (Gerstle et al. 2007).

The peridynamic formulation is based upon Newton's second and third laws, where a group of finite or infinitesimally small particles interact with each other through internal forces called 'pair-wise' force functions (with units of force per unit volume squared). Only particles closer together than the material horizon 'δ' are assumed to interact: particles more distant than this material horizon do not interact. The elastic peridynamic formulation can be expressed as (Silling 1998, Gerstle et al. 2005):

$$\int_R \vec{f}_{ij}(\vec{\eta},\vec{\xi})dV_j + \vec{b}_i = \vec{0} \quad , \tag{1}$$

where for a linear elastic material

$$f_{ij}(\vec{\eta},\vec{\xi}) = c\left(\frac{\left|\vec{\xi}+\vec{\eta}\right|-\left|\vec{\xi}\right|}{\left|\vec{\xi}\right|}\right) = c\,s \tag{2}$$

if $\left|\vec{\xi}\right| < \delta$, and $f_{ij}(\vec{\eta},\vec{\xi}) = 0$ otherwise. $\vec{f}_{ij}(\vec{\eta},\vec{\xi})$ is the pairwise force function (per unit volume squared) between particles '*i*' and '*j*' with volumes dV_i and dV_j respectively, $\vec{\eta}$ and $\vec{\xi}$ are the relative displacement and the relative position between these particles, $\vec{b}_i$ is the externally applied force per unit volume, c is a micro elastic constant, and s is the stretch of the peridynamic link. The above formulation can be extended to the micropolar model by adding moments and relative rotations (Gerstle et al. 2006):

$$\int_R \vec{f}_{ij}(\vec{\eta},\vec{\xi},\vec{\theta})dV_j + \vec{b}_i = \vec{0} \;\text{; and} \tag{3}$$

$$\int_R \vec{m}_{ij}(\vec{\eta},\vec{\xi},\vec{\theta})dV_j + \vec{m}_i = \vec{0} \;, \tag{4}$$

where $\vec{\theta}$ is the relative rotation, $\vec{m}_{ij}$ is the moment function (with units of moment per volume squared), and $\vec{m}_i$ is the externally applied moment per unit volume. At the microelastic level, the pairwise force function $\vec{f}_{ij}$ and pairwise moment function $\vec{m}_{ij}$ between particles i and j can be determined using

$$\{df_{ij}\} = [k_{ij}]\{d_{ij}\}dV_i dV_j \tag{5}$$

where the microelastic stiffness matrix $[k_{ij}]$ is a function of the area *A*, moment of inertia *I*, torsional moment of inertia *2I*, microelastic Young's modulus *E'* and length *L* of the micropolar peridynamic link of axisymmetric cross-section shown in Fig. 1, and $\{d_{ij}\}$ is the displacement vector between particles i and j. The axial and bending stiffnesses of such an element are characterized by two constants $c \equiv E'A$ and $d \equiv E'I$, where E' is a micro-elastic Young's modulus.

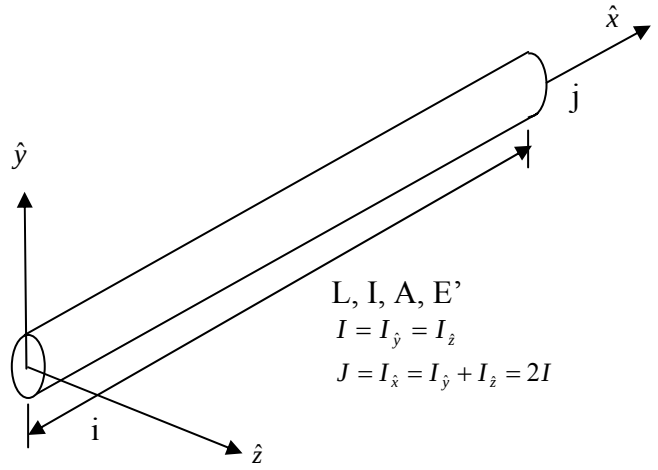

Figure 1. Differential frame element.

The differential strain energy stored in the linear elastic link between particles '*i*' and '*j*' is:

$$dU_{ij} = \frac{1}{2}\lfloor d_{ij} \rfloor \{df_{ij}\} = \frac{1}{2}\lfloor d_{ij} \rfloor [k_{ij}]\{d_{ij}\}dV_i dV_j \;, \tag{6}$$

and the total elastic energy within the domain R is

$$U_R = \frac{1}{4}\int_R \int_R \lfloor d_{ij} \rfloor [k_{ij}]\{d_{ij}\}dV_i dV_j \;. \tag{7}$$

3 FEM IMPLEMENTATION OF MICROPOLAR PERIDYNAMIC MODEL

Using standard finite element interpolation functions, the displacements at any two points '*i*' and '*j*' within elements '*m*' and '*n*', respectively, are:

$$\{d_i\} = [N^m]\{D_m\} \;,\; \{d_j\} = [N^n]\{D_n\}, \tag{8}$$

where $[N^m]$ and $[N^n]$ are the shape function matrices and $[D_m]$ and $[D_n]$ are the element nodal displacements.

The displacement vector for both points '*i*' and '*j*' can be expressed as

$$\{d_{ij}\} = \begin{Bmatrix}\{d_i\}\\ \{d_j\}\end{Bmatrix} = \begin{bmatrix}[N^m]\{D_m\}\\ [N^n]\{D_n\}\end{bmatrix} = \begin{bmatrix}[N^m] & [0]\\ [0] & [N^n]\end{bmatrix}\begin{Bmatrix}\{D_m\}\\ \{D_n\}\end{Bmatrix} = [N^{mn}]\{D_{mn}\}. \quad (9)$$

Similarly, when both points '*i*' and '*j*' lie within element '*m*':

$$\{d_{ij}\} = \begin{Bmatrix}\{d_i\}\\ \{d_j\}\end{Bmatrix} = \begin{bmatrix}[N^m]\{D_m\}\\ [N^m]\{D_m\}\end{bmatrix} = \begin{bmatrix}[N^m]\\ [N^m]\end{bmatrix}\{D_m\} = [N^{mm}]\{D_m\}. \quad (10)$$

The stiffness contribution from links between elements '*m*' and '*n*' can be expressed as:

$$[K_{ij}] = \int_{elemi}\left(\int_{elemj}[N^{mn}]^T[k_{ij}][N^{mn}]dV_j\right)dV_i, \quad (11)$$

and the contribution from links entirely embedded within element '*m*' is given by:

$$[K_{ij}] = \frac{1}{2}\int_{elemi}\left(\int_{elemi}[N^{mm}]^T[k_{ij}][N^{mm}]dV_j\right)dV_i. \quad (12)$$

The factor ½ is removed from Equation (11) to avoid double-counting the matrices $[k_{ij}]$ and $[k_{ji}]$. Following the assembly of the global structure stiffness matrix, the displacements and forces can be determined in the usual manner.

The whole point of casting the peridynamic model within a finite element framework is to reduce the number of simultaneous equations, which must be solved. The finite element method, however, constrains the displacement field to be continuous within finite elements. This constraint is not unreasonable in regimes where peridynamic links are elastic. However, where such links soften or are completely broken, the solution involves strain localization. In such cases, it is necessary to make the finite elements be significantly smaller than the material horizon δ to obtain mesh-independent results.
Note that using the present formulation; it is not necessary to connect elements together at nodes, because the stiffness of the peridynamic links between elements closer together than the material horizon, δ, ensures that correct displacements will be computed. However, in regimes where it is known that localization of strain cannot occur, finite elements can still be connected together at nodes as a means of reducing the number of degrees of freedom.

Also, note that the method works for 1D, 2D, and 3D elements of all types (frames, plates, shells, etc.), and we also do not preclude zero-dimensional (point) finite elements.

Finally, note that as a solution proceeds, it is possible to replace higher-dimensional elements with 0D elements in order to allow strain localizations to proceed unhindered by the assumptions of interpolations within the higher-dimensional elements. However, this will be at the expense of additional degrees of freedom. An example of this type of adaptive solution is presented in Section 7.

The next section explains how, for an elastic domain (far from a boundary), the micro elastic parameters c and d can be determined from the conventional macro elastic Young's modulus *E* and Poisson's ratio ν, thus relating micropolar peridynamics and conventional continuum mechanics-based elasticity theory.

4 RELATIONSHIP BETWEEN MICRO- AND MACRO-ELASTIC CONSTANTS

With reference to Fig. 1, we have defined micro elastic constants $c \equiv E'A$ and $d \equiv E'I$. An expression for the peridynamic strain energy density can be obtained by integrating the energy stored in all peridynamic links expressed by Equation (6) connected to a given differential material point, assuming a uniform principal strain field {ε}. For planar peridynamic links, this expression is given by (Gerstle et al 2006):

$$U = \frac{\pi}{4}\begin{bmatrix}\varepsilon_1 & \varepsilon_2\end{bmatrix}\begin{bmatrix}\frac{c\delta^3}{4}+3\delta d & \frac{c\delta^3}{12}-3\delta d\\ \frac{c\delta^3}{12}-3\delta d & \frac{c\delta^3}{12}+3\delta d\end{bmatrix}\begin{Bmatrix}\varepsilon_1\\ \varepsilon_2\end{Bmatrix}. \quad (13)$$

Likewise, for plane stress conditions, the internal strain energy density using conventional theory of elasticity is given by:

$$U = \frac{1}{2}E\begin{bmatrix}\varepsilon_1 & \varepsilon_2\end{bmatrix}\begin{bmatrix}\frac{1}{(1-\nu)(1+\nu)} & \frac{\nu}{(1-\nu)(1+\nu)}\\ \frac{\nu}{(1-\nu)(1+\nu)} & \frac{1}{(1-\nu)(1+\nu)}\end{bmatrix}\begin{Bmatrix}\varepsilon_1\\ \varepsilon_2\end{Bmatrix}. \quad (14)$$

Because Equations (13) and (14) must be equal for all strain states, {ε}, the micro elastic constants '*c*' and '*d*' can be obtained as functions of the constants *E*, ν, and the material horizon δ:

$$c = \frac{6E}{\pi\delta^3(1-\nu)} \qquad d = \frac{E(3\nu-1)}{6\pi\delta(\nu^2-1)}, \quad (15)$$

and the values of the macroelastic parameters as functions of the microelastic constants are obtained by solving Equations (15):

$$E = \frac{\pi c\delta^3\left(c\delta^2 + 36d\right)}{9\left(c\delta^2 + 12d\right)} \qquad \upsilon = \frac{c\delta^2 - 36d}{3\left(c\delta^2 + 12d\right)}. \qquad (16)$$

Using the same technique, for plane strain conditions the relations are:

$$c = \frac{6E}{\pi\delta^3\left(1-\nu-2\nu^2\right)},\ d = \frac{E\left(1-4\nu\right)}{6\pi\delta\left(1-\nu-2\nu^2\right)} \qquad (17)$$

and

$$E = \frac{\left(c\delta^2 + 36d\right)\left(5c\delta^2 - 36d\right)\pi}{48c\delta}, \upsilon = \frac{c\delta^2 - 36d}{4c\delta^2}. \qquad (18)$$

For the case of uniaxial stress:

$$c = \frac{2E}{\delta^2} \text{ and } E = \frac{c\delta^2}{2}, \qquad (19)$$

and for fully 3D conditions:

$$c = \frac{6E}{\pi\delta^4\left(1-2\nu\right)},\ d = \frac{E\left(1-4\nu\right)}{4\pi\delta^2\left(1-\nu-2\nu^2\right)}, \qquad (20)$$

and

$$E = \frac{\pi\delta^4 c\left(c\delta^2 + 36d\right)}{12\left(c\delta^2 + 6d\right)},\ \nu = \frac{c\delta^2 - 24d}{4\left(c\delta^2 + 6d\right)}. \qquad (21)$$

We next explore an elastic size effect predicted by the micropolar peridynamic theory.

5 ELASTIC SIZE EFFECT

As explained in the previous section, the micropolar peridynamic strain energy density of a given material particle is one-half of the integral of the strain energy stored in the micropolar peridynamic links connected to the particle. For particles further than the material horizon, δ, from a domain boundary, the relationships between c, d, E, and ν are as described in the previous section.

However, Figure 2 shows that a particle can be located at a distance less than the material horizon ($a < \delta$) from a domain boundary. Particles with $a < \delta$ have truncated peridynamic horizons, and thus have fewer micropolar links than particles within an interior region. The peridynamic energy density is determined and assumed to be equal to the strain energy of a transversely isotropic material from the classical theory of elasticity, as shown in Fig. 2. The macro-elastic properties of the peridynamic material are plotted as functions of $\xi \equiv a/\delta$ and of the corresponding elastic properties (E, ν) of an isotropic material in the interior region in Figures 3-6. The notation used is shown in Figure 2.

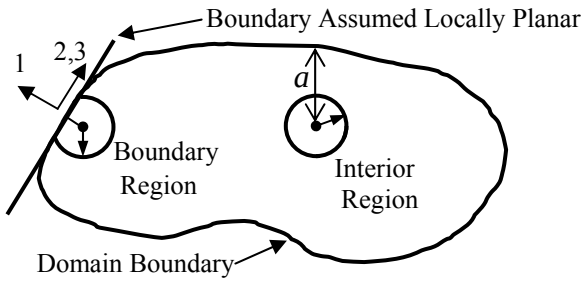

E_1 = *Orthotropic Direction*

$E_2 = E_3$ = *Isotropic Direction*

$$\upsilon_{12} = -\frac{\varepsilon_2}{\varepsilon_1};\quad \upsilon_{23} = -\frac{\varepsilon_3}{\varepsilon_2};\quad \xi = \frac{a}{\delta}$$

Figure 2. Peridynamic interior and boundary regions.

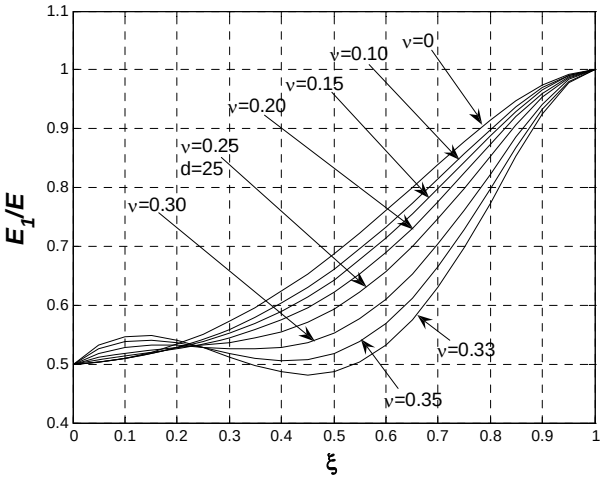

Figure 3. E_1/E versus ξ for varying values of ν.

The fact that the effective Young's modulus is reduced within a boundary layer of thickness δ indicates that as specimen size increases the apparent material stiffness increases. This elastic size effect is significant for small specimen sizes (or at least for specimen sizes not much larger than the peridynamic material horizon, δ). It would be interesting to see if such a size effect can be observed experimentally in concrete.

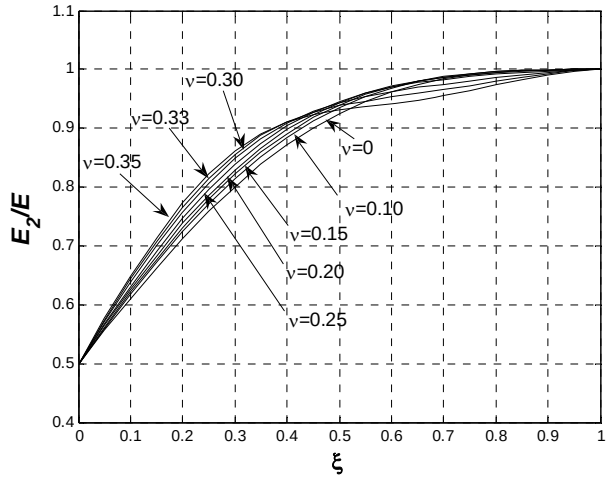

Figure 4. E_2/E versus ξ for varying values of ν.

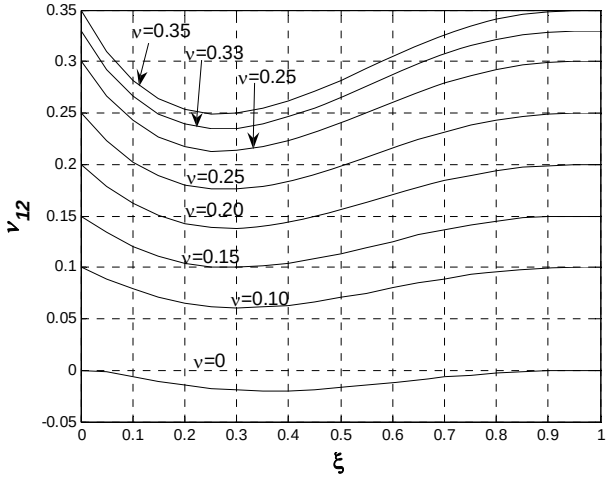

Figure 5. ν_{12} versus ξ for varying values of ν.

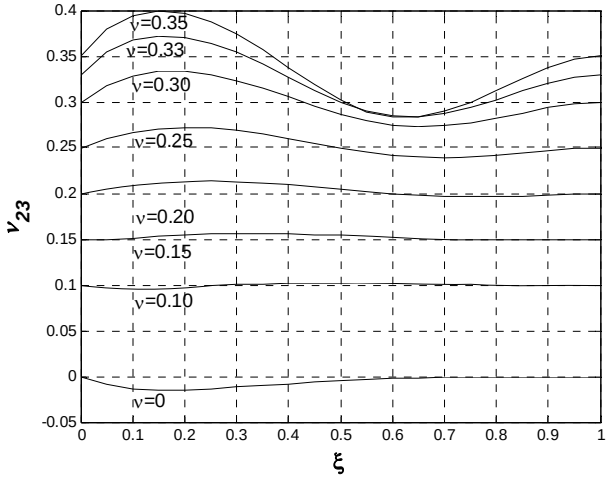

Figure 6. ν_{23} versus ξ for varying values of ν.

6 MICROPOLAR PERIDYNAMIC MODEL FOR CONCRETE UNDER MONOTONIC LOADING

Gerstle & Sau (2004) developed a very simple model for concrete by assuming a peridynamic model with micro elastic stiffness c and a cut-off stretch s*, after which the peridynamic link is broken. This model significantly under-predicted the compression strength and energy absorption capacity of concrete in compression.

We now propose a more accurate micropolar peridynamic model (which is still applicable only to concrete under monotonically increasing or decreasing deformation). In this new model, the stiffness of a given peridynamic link connecting particles *'i'* and *'j'* depends not only upon the axial stretch, s_r, of particles i and j, but also upon the maximum stretch, s_t, of any other peridynamic link connected to particle i.

As shown in Figure 7, the link remains linearly elastic as long as its stretch, s_r, exceeds a compressive limit, s_{comp}. However, if s_r exceeds a specific tensile limit, s_{tens}, the tensile peridynamic force remains constant until s_r exceeds another specific limit, $\alpha_{tens}s_{tens}$, after which the force drops to zero.

On the other hand, if s_r is less than a compressive limit, s_{comp}, two possibilities exist. If the maximum transverse stretch, s_t, is less than s_{tens} the link remains linear elastic, while if s_t, is greater than s_{tens} the compressive force remains constant until s_r exceeds another specific limit, $\alpha_{comp}s_{comp}$, after which it drops to zero.

The sensitivity to the transverse stretch, s_t, arises due loss of lateral support and consequent compressive instability of the peridynamic link. The plateau in the compressive regime simulates energy dissipation due to friction.

To summarize, our micropolar peridynamic model for concrete has seven parameters: c, d, δ, s_{tens}, s_{comp}, α_{tens}, and α_{comp}. Each of these parameters has plausible mechanistic justification at the micro- (or meso-) mechanical level.

As a means of visualizing the results of this model, we have made the simplifying assumption that a spatially uniform principal strain field, $\{\varepsilon_1, \varepsilon_2\}$ exists, with no strain in the third direction.

To model a typical concrete, we select E = 24.85 GPa, ν = 0.22, and δ = 2.54 cm, from which we calculate using Eq. (16) c = 3.713×10^6 GN/m^5 and d = 18.54 GN/m^3. We also select s_{tens}=0.00014 s_{comp}=0.001 α_{tens}=2 and α_{comp}=3. For a uniaxial stress condition this model predicts the stress-strain relations depicted in Figure 8.

For the case of uniaxial plane strain behavior, this model seems to correctly replicate Young's Modulus, Poisson's ratio, tensile strength, compressive strength, fracture toughness, and approximately the correct shape of the compressive stress-strain curve. In addition, biaxial compressive behavior seems to be correctly modeled. Most importantly, the model is capable of objectively predicting strain localizations so that fracturing behavior of specimens of finite size under various loading conditions can be studied.

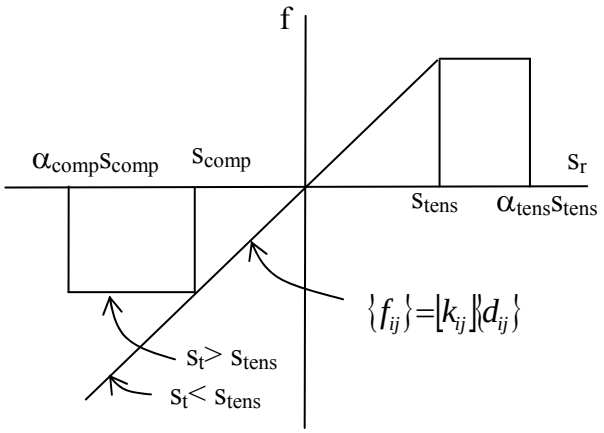

Figure 7. Constitutive Behavior of a Peridynamic Link.

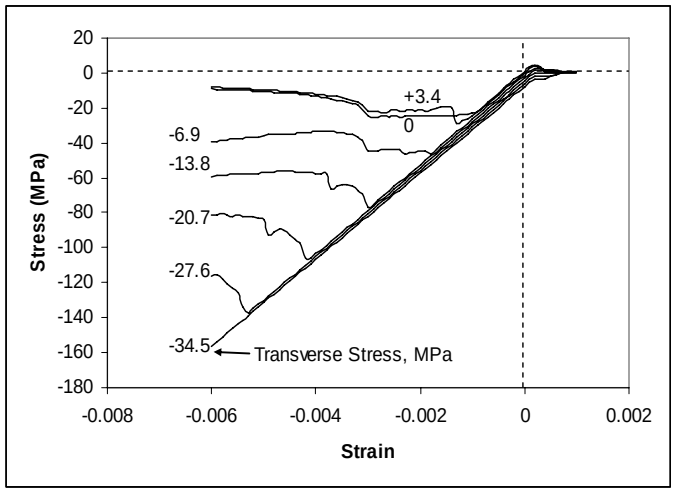

(a) Overview

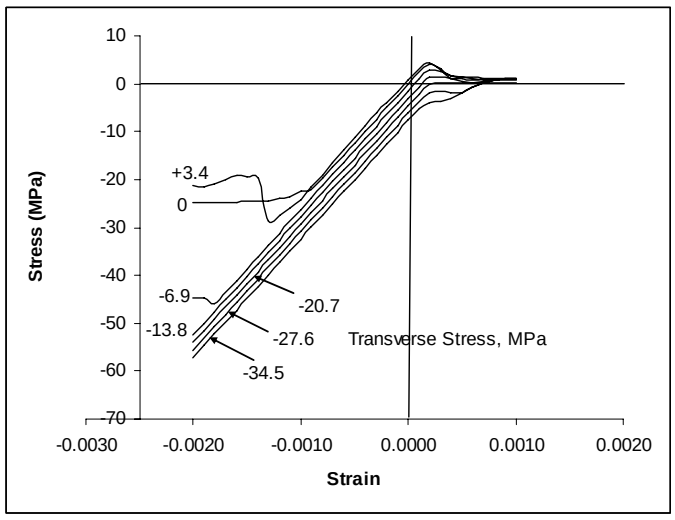

(b) Close Up of Tensile Region

Figure 8. Stress-Strain Relations computed from Plain Strain Micropolar Peridynamic Concrete Model.

7 EXAMPLE

A peridynamic finite element code was developed using MatLab and C++. Using the finite element methodology described in Section 3, damage in concrete is modeled through a simple maximum stretch, s*, tension tension-cutoff (rather than with the more accurate model presented in Section 6). With a maximum principal strain criterion, membrane elements (2D elements) are converted as necessary into 0D elements. Assuming the simplest of microelastic damage models described in Gerstle & Sau (2004), peridynamic links are broken one by one.

Figure 9 shows the results of a simulation of a specimen in tension. The 2D elements are adaptively converted to 0D elements, and then peridynamic links between 0D elements are broken one by one.

The seven-parameter concrete model described in Section 6 has not yet been implemented into the finite element code.

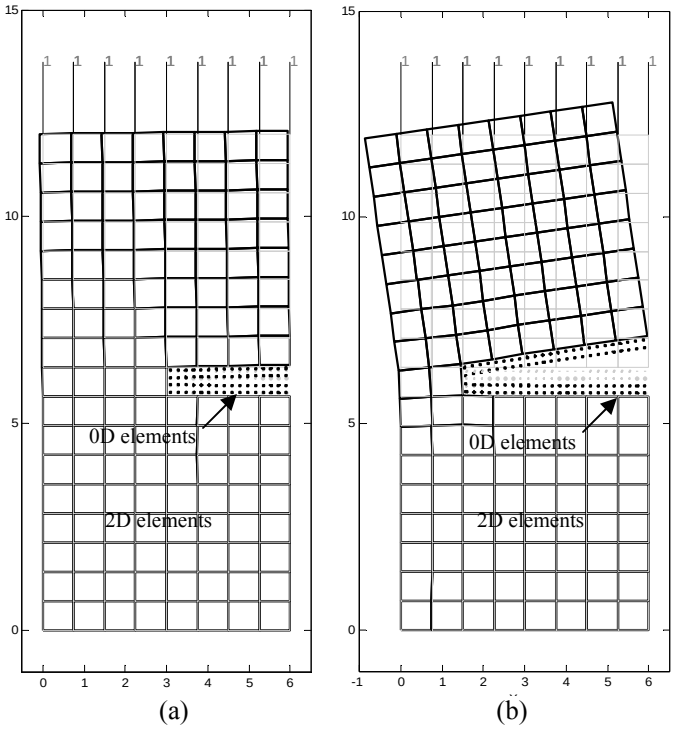

Figure 9. Plain concrete cylinder subjected to tensile load after 75 (a) and 150 damage steps (b).

8 CONCLUSIONS

The micropolar peridynamic model has been presented, as well as a finite element method for efficiently obtaining computational solutions to static problems. In contrast to the original, central force peridynamic model, the micropolar peridynamic model is capable of representing elastic materials with varying Poisson's ratios.

In contrast to classical elasticity, which has two constants E and ν, the presented linear elastic micropolar peridynamic model has three constants: c, d, and δ. The material horizon, δ, can be viewed either as a free parameter that can be chosen for purpose of computational solution, or as a true material constant characterizing the concrete material. In ei-

ther case, the paper has presented the relationships between the classical macro elastic constants E and ν, and the three micropolar peridynamic constants c, d, and δ.

The peridynamic model predicts reduced stiffness near the domain boundary that classical elasticity fails to capture. It would be interesting to determine experimentally whether or not concrete laboratory specimens exhibit this predicted elastic peridynamic size effect.

We have proposed a displacement-based nonlinear micropolar model which, in addition to c, d, and δ, has two tensile (s_{tens} and α_{tens}) and two compressive constants (s_{comp} and α_{comp}), as shown in Figure 7. This model seems to accurately predict the known types of biaxial behavior, including dilatancy, tension-softening and fracture energy in the tensile regime as well as compressive strength and toughness in the compressive regime. The model could be extended to model cyclic and time-dependent behavior as well.

The presented approach has the following virtues:

- conceptual simplicity;
- predicts a testable (but untested) elastic size effect;
- no preconceived assumption of continuity;
- continuity is emergent;
- discrete fracture is emergent;
- distributed damage is emergent;
- relatively efficient computational solution;
- extensible to large-deformation regime;
- extensible to time-dependent regime;
- extensible to represent 3D solid domains, plates, shells, etc.;
- extensible to model reinforced concrete structures, including interaction between steel and concrete.

We intend to explore the micropolar model for concrete in more detail in the coming months and years.

9 ACKNOWLEDGMENTS

The inspiration and support in various forms provided by of Stewart Silling and Michael Hessheimer at Sandia National Laboratories is gratefully acknowledged.

REFERENCES

Gerstle, W. & Sau, N. 2004. Peridynamic Modeling of Concrete Structures. Li, Leung, Willam, & Billington, (eds), Proceedings of the Fifth International Conference on Fracture Mechanics of Concrete Structures, Ia-FRAMCOS, Vol. 2, pp. 949-956.

Gerstle, W., Sau, N., & Silling, S. 2005. Peridynamic Modeling of Plain and Reinforced Concrete Structures. Atomic Energy Press (ed.), 18th Intl. Conf. on Structural Mechanics in Reactor Technology (SMiRT18), August 7-12, 2005 Beijing China.

Gerstle, W., Sau, N. & Silling, S. 2007. Peridynamic Modeling of Plain and Reinforced Concrete Structures. Elsevier (ed.), Nuclear Engineering and Design, accepted, August, 2006.

Schlangen E. & Van Mier, J.G.M 1992.Micromechanical Analysis of Fracture of Concrete. Int. J. Damage Mechanics 1: 435-454.

Silling, S. 1998. Reformation of Elasticity Theory for Discontinuous and Long-Range Forces. SAND98-2176, Sandia National Laboratories, Albuquerque, NM.

Silling, S. 2000. Reformulation of Elasticity Theory for Discontinuities and Long-Range Forces. Journal of the Mechanics and Physics of Solids 48: 175-209.

Silling, S. 2002. Dynamic Fracture Modeling With a Meshfree Peridynamic Code. SAND2002-2959C, Sandia National Laboratories, Albuquerque, NM.